72nd International Astronautical Congress (IAC), Dubai, United Arab Emirates, 25-29 October 2021.

IAC-21,C4,10-C3.5,1,x63502

THRUST MEASUREMENTS OF MICROWAVE-, SUPERCONDUCTING- AND LASER-TYPE EMDRIVES

Oliver Neunzig[a], Marcel Weikert[b], Martin Tajmar[c]

[a] Institute of Aerospace Engineering, Technische Universität Dresden, Marschnerstrasse 32, 01307 Dresden, Germany, oliver.neunzig@tu-dresden.de
[b] Institute of Aerospace Engineering, Technische Universität Dresden, Marschnerstrasse 32, 01307 Dresden, Germany, marcel.weikert@tu-dresden.de
[c] Institute of Aerospace Engineering, Technische Universität Dresden, Marschnerstrasse 32, 01307 Dresden, Germany, martin.tajmar@tu-dresden.de

Abstract

Propellantless propulsion concepts based on electromagnetic waves like the EMDrive are claimed to be far superior with respect to the state of spacecraft propulsion systems. Such devices consist of enclosed cavities with different geometric shapes that are injected with electromagnetic waves, producing unidirectional thrust without expelling propellant. Additional concepts emerged from theories like quantised inertia and involve laser-type EMDrives with optical cavity resonators and fiberoptic loops in the infrared spectrum. Claimed forces of these devices in the micronewton range are confronted with growing scepticism when basic conservation laws are applied. With cutting-edge measurement devices, we were able to characterize these concepts in a space-like environment with nanonewton resolution for thruster masses of up to 10 kg. Additionally, we enhanced our inverted double pendulum thrust balance with the ability to perform thrust measurements at cryogenic temperatures (65 K) to operate also a superconducting EMDrive that was claimed have orders of magnitude higher thrust compared to classical resonators. In this paper, we present changes to each setup, based on criticism to our latest results, as well as thrust measurements of each device. Neither the EMDrive cavities nor the infrared laser resonators created a net-thrust above our balance noise. With the exception of the superconducting EMDrive, our data limits anomalous thrust below the threshold of classical propulsion with photon pressure for equivalent power-levels. Despite the enhancements made to each device, we did not detect any evidence in favour of the proposed theories.

Keywords: Propellantless propulsion, EMDrive, laser resonator, superconductor, thrust balance

Acronyms/Abbreviations
COM – Center of mass
SC – Superconductor
EM – Electromagnetic
YBCO – Yttrium-Barium-Copper-Oxide
QI – Quantised Inertia

1. Introduction

The reliance of modern propulsion systems on propellant puts strong limits on their ability to perform large-scale space exploration. So far, the ultimate propellantless propulsion concept is pure photon pressure, e.g. produced by a laser. Solutions to break through this limit may hide in yet unknown interactions of fundamental properties like mass and inertia. The emergence of novel theories and concepts that allow experimental research of propulsion candidates is an important aspect to reach this goal.

Some of these theories predict forces in the μN range and also well above for attainable power-levels in a laboratory environment. Our goal is to develop advanced testing facilities, manufacture promising thruster candidates and characterized them in order to find out if they work as promised.

We recently reported results of a thorough test campaign to characterise both the so-called EMDrive [1], which uses microwaves inside a copper resonator, as well as Laser-EMDrive [2], which uses optical resonators in various different configurations. During our tests we could reproduce forces on our balance that were similar to the ones reported by others or claimed by some of the proposed theories, however, our measurements also revealed that their origin was not real but linked to a number of setup-related issues like thermal-induced mechanical stress on the balance. Once all thrusters were properly mounted, all false-positives disappeared and all measurements were below the equivalent photon thrust limit considering the power levels used.

After receiving criticism from the advocators of both concepts [3, 4], in this paper we will implement all the requested changes and even expand the capabilities of our thrust balance:

Instead of using an EMDrive cavity with flat end caps and a dielectric disc inside like the one published by

NASA [5], we removed the dielectric and used spherical end caps.

Next, we implemented the capability to cool thrusters to cryogenic temperatures on the balance while retaining µN thrust resolution. This enabled us to test an EMDrive with superconducting end caps that should greatly enhance its thrust.

Lastly, we implemented several setup changes to the laser cavities to test various suggestions of why we obtained a null result.

2. Testing environment

Thrust measurements in the sub-µN regime require the detection of environmentally induced effects that may lead to false-positive thrust signals. These false-positives are often indistinguishable from real thrust and therefore difficult to detect in the first place. We observed and decreased the most influential errors induced by electromagnetic interactions with external magnetic fields in close vicinity, thermal interactions with the thrust balance and especially atmospheric convection. Each individual test series presented in the following chapters was exposed to the same environmental conditions for comparability. Tests took place inside our cylindrical vacuum chamber with an inner diameter of 0.9 m, a length of 1.5 m and a minimum operating pressure in the region of 10e-7 mbar with a *Pfeiffer* Turbopump supported by an *Edwards* scroll pump. The vacuum chamber features its own concrete basis that is separated from the lab building to decrease seismic noise to the thrust balance. Continuous enhancements in decreasing environmental influences enabled us to reach the desired thrust noise benchmark of photon pressure. This means, that we are able to compare each thrust concept with its operating power level to the equivalent thrust if we converted the same power directly into a beam of photons. Devices under test must exceed this threshold to be of significant interest for space propulsion applications.

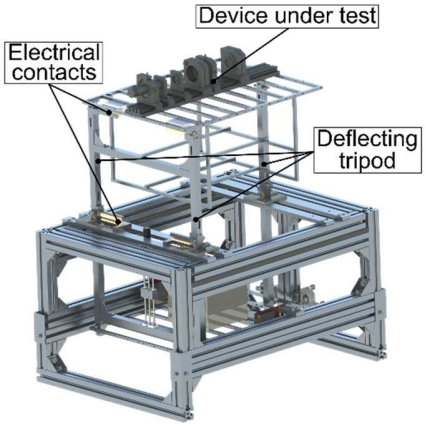

Fig. 1: CAD-rendering of the inverted counterbalanced double-pendulum thrust balance developed at TU Dresden.

An important part of the high thrust resolution was the development of a thrust balance based on an inverted counterbalanced double pendulum (fig. 1). The measurement principle includes a deflecting frame onto which thrusters apply a force that linearly deflects a spring-mounted parallelogram (fig. 2). The deflection is measured with an *attocube IDS3010* Interferometer and converted into thrust values by previously characterizing the correlation between spring deflection and applied forces. The balance is able to detect the continuous force of a 0.5 W steady-state laser, which translates to 1.67 nN with a thrust-to-noise ratio of 10 and can support thruster masses of up to 10 kg.

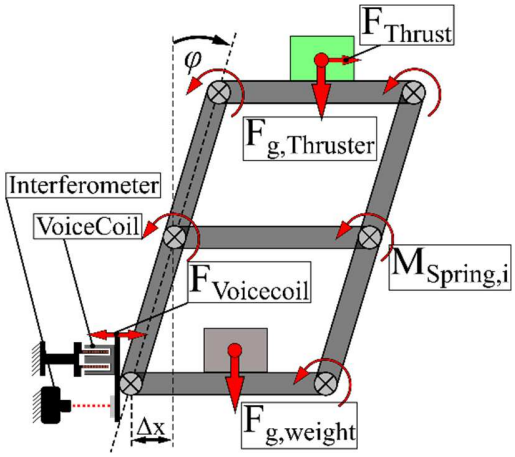

Fig. 2: Measurement principle of the inverted double-pendulum thrust balance.

Setups with laser-resonators operated in a vacuum level of 10e-6 mbar due to the low laser power levels and therefore high-resolution requirements. This vacuum level also reduces false thrust signatures from outgassing components that may occur due to heat generation from the impacting laser beam.

The EMDrive with a spherical endcap operated in the same vacuum chamber at a higher pressure of 10e-2 mbar as it was sufficient for the desired thrust noise. The superconducting version of the EMDrive on the other hand required the usage of liquid and solid nitrogen as a coolant. The measurement process and environmental pressure with a nitrogen gas generator will be discussed in a later section of this paper.

Prior to each set of measurements the thrust balance is calibrated to ensure unaltered operating conditions. By applying consecutive forces of different magnitudes with a voicecoil, we characterize the correlation between applied force and resulting balance deflection with statistical significance. Each data point is transferred into a linear fit of commaned force against measured displacement to verify linear deflective behaviour of the torsional springs. The so-called calibration factor, usually

in the range of 1 µN/µm, is used to convert displacements into corresponding thrust values.

Thermal drifts due to heat generation on the balance are always present and superimposed on the thrust signal. As long as the drift is within a tolerable magnitude, we use software tools with LabView to automatically remove them. Every thrust measurement presented in the following subsections is an average of consecutive measurements with the same operating parameters to further decrease the balance resolution and highlight the existence of force plateaus.

A summary of every measured thrust value, discussed in the following chapters, is presented in appendix B.

3. Microwave EMDrive

The EMDrive is a tapered resonant cavity operated with electromagnetic waves in the microwave spectrum. Microwaves resonating back and forth inside the tapered resonator are proposed to exceed a significant net-force due to a difference in radiation pressure between both end-plates.

In a recent publication [1] we presented our approach to manufacture and operate the EMDrive similar to the cavity tested at the NASA Eagleworks laboratory, as it is the first peer-reviewed measurement of an EMDrive with a positive thrust result. We identified and eliminated several measurement influences that result in false-positive thrust effects with the same signature as seen by White et al [2]. The predominant influence included thermally induced center of mass (COM) shifts that create convincing thrust signatures. These signatures are often misinterpreted as real thrust in torsion balance measurements, like the ones used by NASA. After eliminating the influences, we attained a thrust resolution that was below the equivalent photon-pressure threshold and our latest thrust measurements [1] did not reveal any thrust above balance noise originating from the NASA-like cavity. For the cavity presented in this paper, we made several setup changes to gain the desired operating conditions, as suggested by Shawyer [6].

3.1 EMDrive - Experimental Setup

The device used the same cavity geometry utilized in previous tests [1], but we replaced the flat end plate on the larger side with a spherical end-cap and removed the dielectric (HDPE) within the cavity entirely to reduce the phase deviation described by Shawyer [6]. The small endcap remained flat and has a tight fit within the cylindrical flange of the cavity that allows fine-tuning. Geometric dimensions of the cavity are shown in figure 3. Furthermore, we increased the quality factor of the cavity at important resonant frequencies to further increase predicted force values.

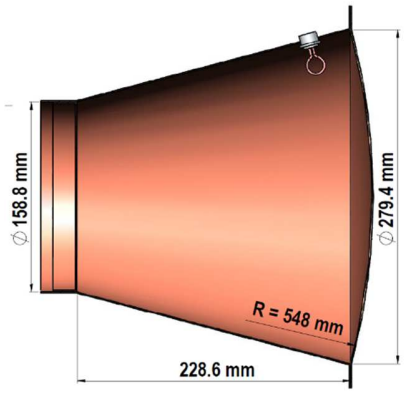

Fig. 3: Geometrical dimensions of the copper cavity with a spherical end-cap at the large diameter.

For the electrical setup, we operated the EMDrive in the same manner as before with an on-board battery-pack with six Lithium-Ion cells and balancing electronics for recharging to supply the microwave amplifier without the need for electrical feedthroughs on the balance. We utilized the liquid metal feedthroughs solely for data acquisition as they would interfere with thrust measurements otherwise. Additionally the electrical setup on the balance, as seen in appendix A, figure 21, contained the following components:

-Mini Circuits ZX95-2041-S + voltage-controlled frequency generator
-Mini Circuits ZX73-2500-S + voltage-controlled attenuator to control the output power of the amplifier
-EMPower SKU 1164 RF solid-state amplifier with a maximum output power of 50 W and an amplification of 47 dB
-MECA CN-1.950 circulator to prevent damage to the amplifier from reflected power
-Mini Circuits BW-N30W20 + fixed attenuator
-Mini Circuits XZ47-40LN-S + power meter
-Maury Microwave 1878B three-stub tuner for impedance matching directly coupled to the feed antenna

A major difference to our previous tests is the attachment of a sensing antenna to the cavity with an N-Type connector. The antenna is located near the small end cap and positioned 90° relative to the feed antenna position. It serves as an indicator for microwave power being present inside the cavity. However, the absolute power value cannot be determined with the sense antenna, because the power at the antenna position is mode-dependent. The electrical setup consumed up to 100 W of power during operation on the balance, which is a considerable amount of heat generation on the balance that may interfere with measurements.

For tuning purposes, we used an Anritsu MS46121A single-port Vector Network Analyzer. The additional sensing antenna allowed a more precise tuning process with a two-port analyser. In this way, the important power transmission S21 through the cavity could be determined.

Our thrust measurements involved four resonance frequencies ranging between 1918 MHz and 2054 MHz with loaded Q values of up to 1027.

3.2 EMDrive – Results & Discussion

Our previous measurement campaigns with the NASA-like cavity revealed numerous influences that created convincing thrust signatures. We identified the mounting position of the cavity on the balance as the most influential source of these false positive thrust effects. For comparability, the cavity presented in this paper was mounted and operated in the same manner as the tests with the NASE-like cavity. The EMDrive was mounted to the upper balance platform in a hanging position using two bearings with bolts that allowed for deflections in the horizontal direction (fig. 4). The hanging setup contained the cavity and every electrical component that is required to operate it. This way, heat generation and therefore COM switches from thermally expanding components occur isolated on the hanging setup. Most micronewton thrust measurement principles are sensitive to COM switches to a certain degree. By isolating these kind of deflections from the measurement axis, our tests gained a large enhancement in sensitivity even though we generated high thermal stress on the device under test.

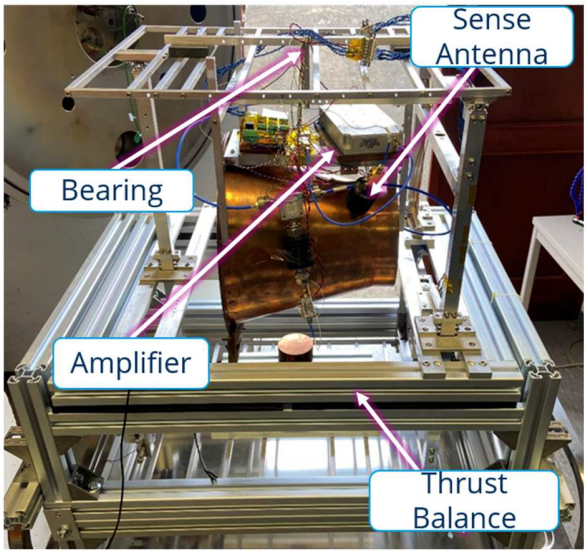

Fig. 4: Measurement setup of the EMDrive mounted to the thrust balance with a bearing suspension hanging from the upper platform.

We identified four resonance frequencies in the bandwidth between 1900 MHz and 2100 MHz (appendix A, fig 23). Power measurements of the sense antenna are presented in figure 22 as well, but as mentioned before, this is not an absolute value for the power in the cavity as it is mode dependent.

Thrust measurements were performed for each of the four resonance frequencies at 1918 MHz, 1946 MHz, 2030 MHz and 2054 MHz with corresponding loaded-Q values and modes summarized in table 1. By using worst-case assumptions and the simplified equations without geometric adjustments, the predicted force values reached up to 22.5 µN for the power levels used, but each thrust measurement at either of the resonance frequencies resulted in balance noise only. Furthermore, the balance resolution during measurements reached values that excluded thrust generation of the EMDrive above its equivalent photon pressure for the given amount of power (Q=1) despite Q-values of several hundreds.

Table 1: Detected resonance frequencies of the EMDrive cavity with corresponding loaded Q-values and their modes.

Resonance Frequency	$Q_{Loaded,S11}$	Mode
1918 MHz	113	Hybrid
1945 MHz	486	TM 210
2030 MHz	677	TE 113
2054 MHz	1027	TE 020

Another claim by the inventor is the necessity of a constant force that counteracts the EMDrive motion, the so-called preload [6]. Although this violates the classical conservation of momentum, this preload is supposed to withhold the cavity motion to store up potential energy within the device and release it as kinetic energy after reaching a certain threshold. An important aspect is the absolute value of this preload, because it must be below the predicted force values. We realised the preload in our setup by commanding forces with the voicecoil, used for calibrations, while the EMDrive was operating. This way the EMDrive experiences a counteracting force with a defined magnitude in either direction. If the preload works as intended, the measured thrust should exceed the commanded thrust by a not-clearly defined amount. With predicted thrust values of several tens of micronewton, we decided to command a preload of ±10 µN and compare it to a balance calibration of ±10µN while the EMDrive was not operating. We tested the preload for each of the four resonant frequencies in both directions. The results are presented in appendix A, figure 25. None of the resonant frequencies responded to the preload and there was no difference in measured thrust while the EMDrive operated. Although we counteracted the cavity motion, it did not release any stored up kinetic energy.

In summary, the cavity with a spherical endcap and no dielectric did not produce any thrust above our balance noise.

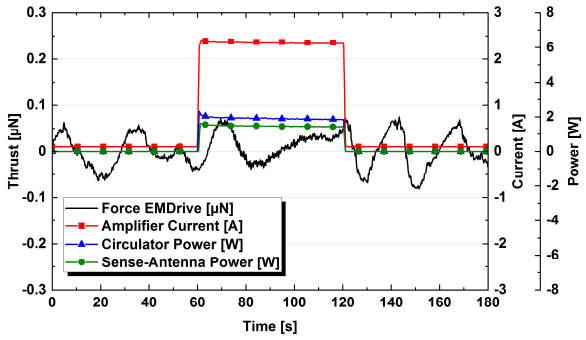

Fig. 5: Thrust measurement of the EMDrive with a spherical end-cap at 1918 MHz resonance frequency. The operating condition is indicated by the amplifier current.

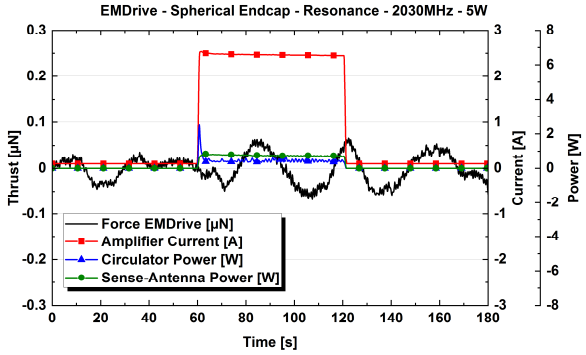

Fig. 6: Thrust measurement of the EMDrive with a spherical end-cap at 2030 MHz resonance frequency. The operating device is indicated by the amplifier current

4. Superconducting EMDrive

The quality factor of a microwave cavity strongly depends on the electrical conductivity of the cavity end-plates. The higher the conductivity, the lower the power loss with each reflection of the electromagnetic wave. According to Shawyer the highest performance of an EMDrive involved superconducting end-caps, enabling quality factors that are orders of magnitude above pure copper end caps [6, 7]. A superconductor is a material with no electrical resistivity when cooled below its so-called critical temperature T_c. This leads to advantageous properties in reflecting electromagnetic waves and boosts the predicted force values of an EMDrive. Shawyer claims extraordinary thrust performance with his so-called 3rd generation EMDrive utilizing YBCO high-temperature superconductors instead of copper [6].

4.1 Superconducting EMDrive - Experimental Setup

We manufactured our own version of a superconducting cavity by using a copper cylinder with a diameter of 160 mm and a length of 210 mm. Copper end-plates are tightly fit into the flanges on each side of the cylinder (fig 7). Two sapphire substrates with a thin film of YBCO coating were mounted on each end plate. A HDPE disc with a thickness of 40 mm was pressed against one of the YBCO substrates to access the desired resonant modes. The assembled cavity was then mounted inside a milled Polystyrene (XPS) box that served as a reservoir for liquid nitrogen while cooling the whole cavity below the critical temperature. Remaining gaps between the XPS and the cavity were sealed using *STYCAST FT2850* cryogenic epoxy with the *24LV* catalyst. For better thermal conductivity between the copper caps and the superconducting waver, we used Apiezon N cryogenic vacuum grease and a 3D printed PEEK structure to press the waver against the copper surface.

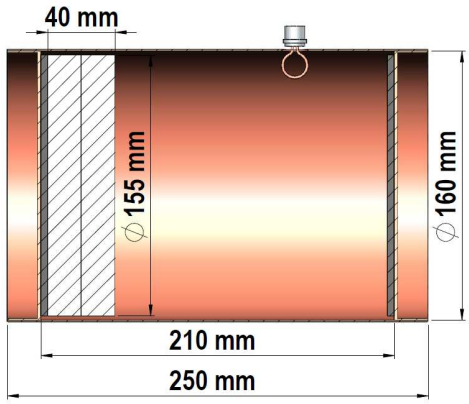

Fig. 7: Geometrical dimensions of the copper cavity with superconductors on each end with a dielectric (HDPE) in-between.

The usage of liquid nitrogen as a coolant introduces various difficulties with the operating electronics, as most of the components are not suitable for cryogenic temperatures. We therefore decided to change the setup in a way that none of the HF-components are exposed to the cryogenic cavity. This was possible by separating the feed antenna physically from the cavity. The Antenna was mounted next to the thrust balance on a rigid structure and submerged into the superconducting cavity that was placed on the moving platform of the thrust balance. There was no mechanical contact between the cavity and the feed antenna. For cavity tuning purposes, we mounted the antenna to a micrometer-linear stage for precise alignments. The miniscule movements during thrust measurements between antenna and cavity in the sub-µm range did not interfere with the cavity tuning. This allowed us to feed the cavity with power from the

outside of the vacuum chamber contrary to the EMDrive setup with the spherical endcap. The electrical setup, as shown in appendix A, fig. 22, involved a *Rigol DSG2011Z* frequency generator, amplified with the *EMPower SKU 1164 RF* solid-state amplifier.

Another challenge of this superconducting cavity is an increased complexity when it comes to thrust measurements. YBCO has a critical temperature of 92 K, which means, that the end caps must stay at cryogenic temperatures with liquid nitrogen (77 K) while mounted to a temperature-sensitive test-bed. We fed the XPS reservoir with liquid nitrogen from a dewar outside of the vacuum chamber. To prevent air-humidity from condensing and forming ice on the thrust balance, we lowered the pressure to 10e-1 mbar inside the chamber. Afterwards, we utilized a LN_2 condenser to fill the vacuum chamber with nitrogen gas until it reaches its triple point at a pressure of 125 mbar. Below this pressure value, nitrogen exists in the form of solid ice that prevents the liquid from entering the reservoir. We then filled the reservoir to create a nitrogen bath around the copper cavity and cool the superconducting end-plates below its critical temperature. Five K-thermocouples indicate the filling level and monitor the temperature of the superconductors. After reaching the superconducting state, we reduced the chamber pressure again to 10e-1 mbar to exploit the solid aggregate state of nitrogen for thrust measurements. Liquid nitrogen or liquids with low viscosity in general on a thrust balance add undesired oscillations through boiling and fluid motion, hence increasing the noise. By lowering the pressure around the XPS reservoir, the liquid bath solidifies and interrupts the fluid motion. As a side effect, the transition from liquid to solid further decreases the temperature by 15 K, which supports the superconducting state. Thrust measurements took place in this environment although solid nitrogen is still able to transition into the gas phase when heated, which creates undesired cold gas thrust in undefined directions.

4.2 Superconducting EMDrive – Results & Discussion

Thrust measurements for the superconducting cavity were performed below and above the critical temperature T_c of the SC to directly compare the influence of superconducting end-caps. The XPS-box, containing the cavity, was mounted on the upper platform of the thrust balance (fig. 8). The advantage of an adjustable measurement range and resolution with our thrust balance was a slight disadvantage for this specific setup. The balance reacts on mass changes on the measurement platform by increasing the calibration factor, which is linked to the sensitivity. This leads to a slight degrade in thrust resolution while the nitrogen-ice evaporates during heat generation. We therefore performed short calibrations in-between each measurement to account for this effect. Furthermore, the stored amount of nitrogen ice within the reservoir limited the available measurement time to around 30 minutes per filling. Although we prevented liquid motion by creating nitrogen-ice, evaporation still interfered with measurements and increased the thrust noise.

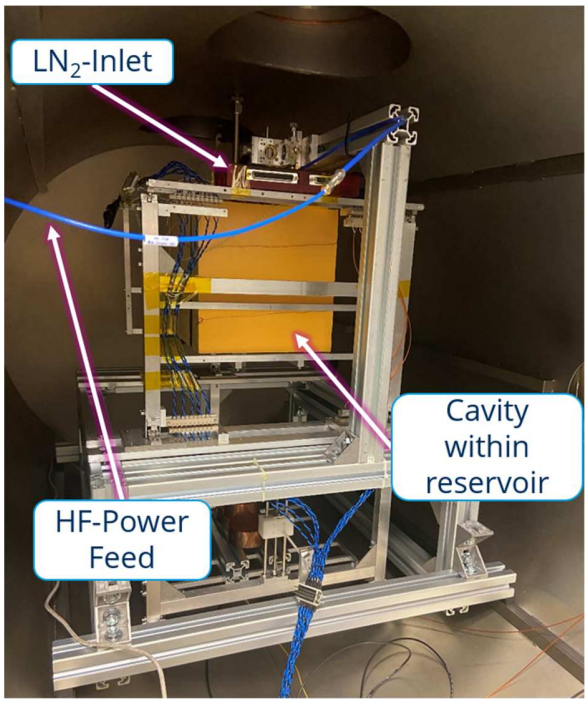

Fig. 8: The superconducting EMDrive within the XPS-reservoir mounted to the thrust balance inside our vacuum chamber.

Within a bandwidth between 1800 MHz and 2000 MHz, we tuned the cavity for at least one resonance frequency at room temperature and scanned an even larger bandwidth for additional frequencies that should emerge after cooling the cavity below T_c. First tests involved the cavity with the dielectric positioned in close vicinity to one of the SC-substrates. Unfortunately, the scanned bandwidth did not reveal additional resonance frequencies after the T_c transition, as shown in the comparison in appendix A, fig. 25. While the tuned resonance frequency at 1843 MHz was still present, no additional peaks arised from the SC. Subsequent cavity tuning efforts did not improve the situation.

Nonetheless, we performed thrust measurements, including the dielectric, at different temperatures. The results are presented in figure 9 with a comparison between measured thrust below and above T_c at the resonance frequency of 1843 MHz. Because the cavity was mounted in a way that showed false positive thrust signatures in previous tests with high calibration-factors [1], similar signatures appeared. Hanging the cavity from a single suspension point like the non-SC cavity was not possible for this setup.

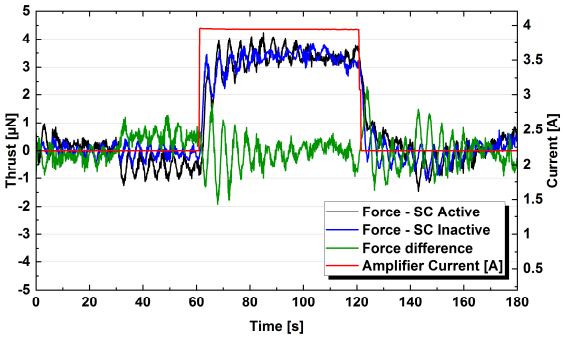

Fig. 9: Thrust comparison of the superconducting cavity with HDPE below and above the critical temperature.

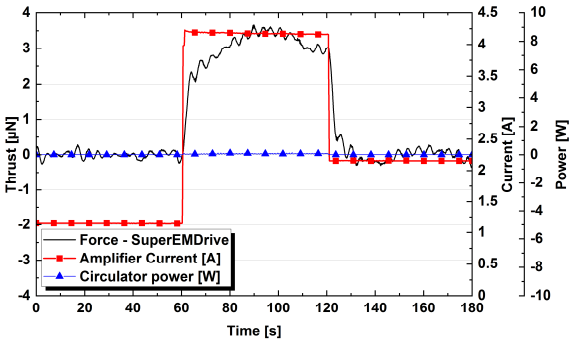

Figure 10: Thrust measurement of the superconducting cavity with HDPE reoriented by 180°.

Inconvenient nitrogen evaporation may be another source that was responsible for the signature. However, the direct comparison between both measurements revealed no effects upon reaching the critical temperature. The superconductors had no influence.

To verify the thrust signal we reoriented the device by 180° and repeated the thrust measurement with same operating conditions below the critical temperature. As seen in fig. 10 the resulting thrust had a similar value and did not change direction. Considering both cases, the thrust signature with HDPE is most likely a measurement artefact.

We suspected that the dielectric was responsible for the absent resonance frequencies below Tc and therefore removed it and retested the cavity in addition with a lower calibration factor of the balance. As seen in appendix A, figure 26, additional resonance frequencies occurred at 1819 MHz and 1959 MHz that were only present below T_c without the HDPE disk. These narrow SC-peaks were characterized by loaded Q-values of 2600 at 1819 MHz and 2063 at 1959 MHz. Corresponding thrust measurements at both resonance frequencies below T_c are presented in figure 11 and 12. For 20 W of commanded power, we detected no thrust effects above the balance noise at both SC resonance frequencies.

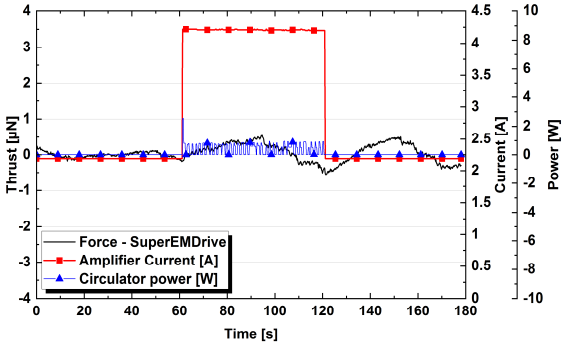

Fig. 11: Thrust measurement of the superconducting cavity without HDPE at 1819 MHz SC-resonance frequency at -202°C with 20 W of commanded power.

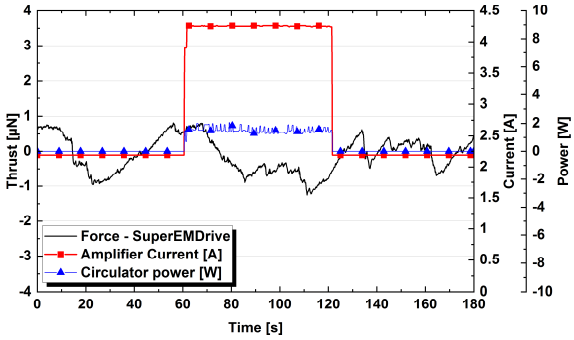

Fig. 12: Thrust measurement of the superconducting cavity without HDPE at 1959 MHz SC-resonance frequency at -196°C with 20 W of commanded power.

5. Laser-Type EMDrive

A more compact form of an EMDrive, as suggested by Taylor, involves electromagnetic waves in the infrared spectrum and optical resonators with lasers rather than microwaves [8]. Taylor bases his ideas on the theory of quantised inertia by McCulloch [9, 10, 11]. In a recent paper [2] we presented our results of an experimental investigation on QI-Theory with optical resonators. QI-Theory claims to describe the origin of inertia with a Modified inertia Hubble-scale Casimir effect (MiHsC). In this model, inertia of an object emerges from damping of Unruh radiation while it experiences acceleration. To explain the origin of inertia McCulloch assumes the formation of a relativistic Rindler horizon appearing in the opposite direction to its acceleration that damps certain wavelengths of the Unruh waves thus creating an inhomogeneous distribution of radiation pressure. This process results in the effect we perceive as inertia with a modified inertial mass m_i, including the standard inertial mass m, the speed of light c, the diameter of the observable universe Θ and the magnitude of acceleration of the object compared to the surrounding matter $|a|$and is given by

$$m_i = m\left(1 - \frac{2c^2}{|a|\Theta}\right)) \quad (1)$$

In a laboratory environment, acceleration of regular masses are so low that this effect only appears cosmic scales. QI's key assumption, however, involve photons at the speed of light instead of regular masses resonating back and forth between reflective surfaces of a laser cavity. Photons supposedly perceive acceleration with each reflection and therefore creating Unruh radiation that can be damped by placing an electrically conductive metal-plate in close vicinity of the reflective surface.

Photons themselves carry momentum that can exchange with surfaces and produce a force F_{Photon} according to equation (2) for full photon absorption where P is the power of a laser beam and c the speed of light. The most important part of the prediction according quantized inertia is an additional factor S that leads to the simplified equation (3) without geometric properties included.

$$F_{Photon} = \frac{P}{c} \tag{2}$$

$$F_{QI} = \frac{PS}{c} \tag{3}$$

The factor S represents the number of reflections inside the optical resonator, the so-called force amplification factor. From this equation, it appears that the produced thrust is given by the classical radiation pressure multiplied by the number of reflection inside each resonator. In the classical interpretation of this experiment, a laser beam resonating back and forth inside an enclosed containment should only produce heat and miniscule mechanical oscillations of the cavity rather than amplified thrust in one direction as it contradicts Newton's action-reaction principle.

The goal of the past test series was thrust measurements with high S-values to compare the data to a beam trap that absorbs the photons on the balance rather than resonate the beam prior to absorption. Recent criticism by McCulloch on our reported negative thrust results and resonator setups lead us to change specific setups according to his suggestions [8].

5.1 Silver Cavity Resonators – Experimental Setup

We previously tested a variety of metal cavity resonators with different geometries and reflectivities made from copper and silver, but no abnormal thrust above the photon pressure was found [2]. The resonators were initially milled from copper and polished to gain a measured reflectivity of approximately 89%, which translates to a force amplification factor of 9 for the used 808nm laser wavelength. To compare each of the three resonators with a different amplification factor, we electroplated the exact same resonators with a thin layer of pure silver, leading to an enhanced reflectivity of 97.5%, thus an amplification factor of 39. The three geometries were named *CC/CX* (concave/convex), *CC/CC* (concave/concave) and *CIRCLE* according to their respective geometry.

The laser source was a modular diode-pumped solid-state laser-kit by *Leybold*. The laser emits a fixed wavelength of 808 nm with adjustable power-levels between 0.01 W and 0.65 W. It is supported by Peltier elements for temperature-controlled wavelength stabilization even in vacuum.

For accurate force predictions and comparability between each setup, we used a *Coherent LaserCheck* power-meter to measure the laser power prior to entering each resonator. The powermeter offers a maximum detectable power of 1 W for wavelengths between 400 nm and 1064 nm with a resolution of 0.01 µW.

The thrust measurements took place by positioning each resonators on the balance that is targeted by a laser source next to the balance on a rigid structure. This way we would expect pure photon thrust at least because the photons are absorbed on the balance and transferring all their momentum to the mounted cavity.

According to McCulloch the resonators should have never been able to generate thrust due to an aluminium plate being present that supposedly prevents Unruh radiation to interact as intended [4]. In our setup, the plate served as a protection against low-power side coils of the laser beam that may affect the temperature sensitive balance components and create false-positive thrust signals. We removed the aluminium case from the cavity and retested each of the three resonators with otherwise equal operating conditions.

5.2 Silver Cavity Resonators – Results & Discussion

Prior to each measurement we made sure that the laser enters the cavities by using an infrared sensitive camera and a *Coherent LaserCheck* powermeter. As an example, the illuminated cavity CC/CX is shown in figure 13. After the laser alignment, the cavities were closed with a polished silver lid to prevent scattered laser power from escaping the cavity. The only setup change of removing the aluminium plate did not have any effect on measured thrust whatsoever.

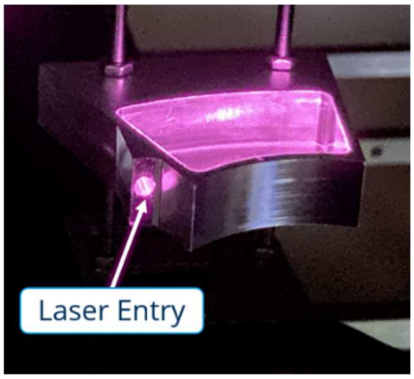

Fig. 13: The illuminated cavity CC/CX on the thrust balance.

Thrust measurements of every cavity for an input power of 467 mW resulted in pure photon thrust (S=1). No anomalous thrust was found nor suppressed by the aluminium plate used in previous tests, as seen in the exemplary thrust measurement in figure 14 and the summarized thrust values in appendix B, table 1.

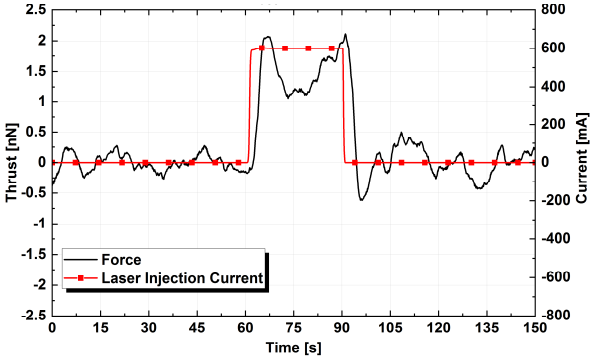

Fig. 14: Exemplary thrust measurement of the CC/CX resonator for a measured laser power of 467 mW.

5.3 Taylor Resonator – Experimental Setup

Additional tests involved high-finesse optical resonators, following the ideas of Taylor [8], to increase the number of reflections by several orders of magnitude compared to the silver cavities. These resonators utilized an asymmetric beam trajectory between two mirrors, originating from Nd:YAG crystals in between that convert the initial laser wavelength of 808 nm to 1064 nm while widening the beam (appendix A, fig. 28). For this setup, we used the same *Leybold* solid-state laser-kit, extended with highly reflective mirrors from *Laser Components* as well as the *Coherent* powermeter to measure the laser power before entering the resonator.

The resonators reached up to 1000 internal reflections (S-value) and increased force predictions by many orders of magnitude according to eq. (3). No anomalous thrust was detected in any configuration [2].

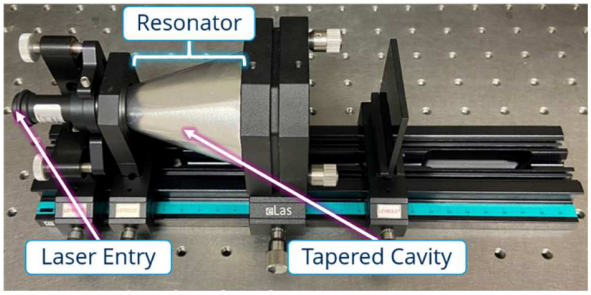

Fig. 15: The Taylor setup enhanced by a tapered metal cavity and a metal end-plate surrounding the laser beam trajectory.

However, according to recent criticism by McCulloch these setups should have never produced thrust because the beam requires an asymmetric metal cavity surrounding the laser beam [4]. Therefore, we manufactured an aluminium cone and encapsulated the beam trajectory of the Taylor-light setup completely with an additional aluminium endcap at the resonator exit (fig. 15).

5.4 Taylor Resonator – Results & Discussion

The addition of an electrically conductive metal cone around the laser beam trajectory in combination with a metal end plate made the confirmation of a stable resonator more difficult. An active resonator is indicated by the conversion of the initial 808 nm wavelength into 1064 nm due to the half-mirrored Nd:YAG crystal. The opposed mirror is permeable for the very low power fraction of the 1064 nm wavelength that manages to penetrate the highly reflective mirrors. This fractional laser power escapes the resonator and hits an infrared sensitive detection card to verify the active resonator. After this procedure, the aluminium end plated is mounted to the backside of the mirror to completely encapsulate the beam trajectory.

Thrust measurements at two power levels of 289 mW and 493 mW resulted in pure photon thrust (S=1) despite predicted thrust values that were magnitudes above the balance noise. No anomalous thrust was detected in presence of a tapered aluminium cone around the laser beam, as seen in an exemplary thrust measurement in fig 16 and the summarized thrust data in appendix B.

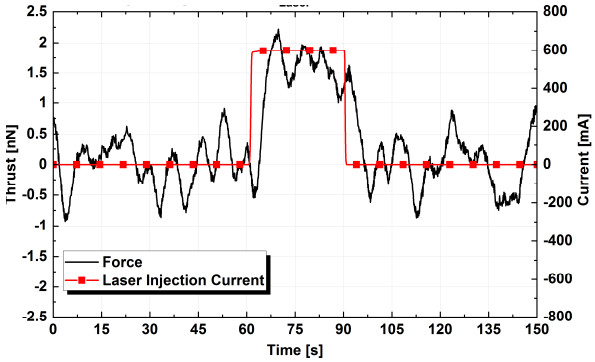

Fig. 16: Thrust measurement of the Taylor-Setup for a measured laser power of 493 mW with an added tapered metal-cone surrounding the laser beam.

5.5 Fiberoptic Loop – Experimental Setup

The third type of photon based resonators, that was subject to tests, is a fiber-optic loop. By feeding a laser into several windings of fiber-optic wire, the travelling photons perceive a change in acceleration relative to the surrounding matter while changing direction, according to QI-Theory. In contrast to the metal cavity resonators, the fiber-optic loop possesses an accurately defined value for the force amplification factor S of up to 3300, that is determined by the number of windings. This advantage enables very accurate force predictions according to eq.

(3). The emerging Rindler horizon of the accelerated photons were substituted with an artificial horizon in the shape of an aluminium plate positioned close to loop windings. This artificial horizon should dampen the emerging Unruh radiation asymmetrically, leading to a unidirectional force (fig 17). The asymmetric loop retested in this measurement series utilized 2.2 km of multimode fiber wound around a 3D-printed Polyetheretherketone (PEEK) mount with a radius of 70 mm on the big end and 40 mm on the small end. The centre points of each radii are 150 mm apart from each other.

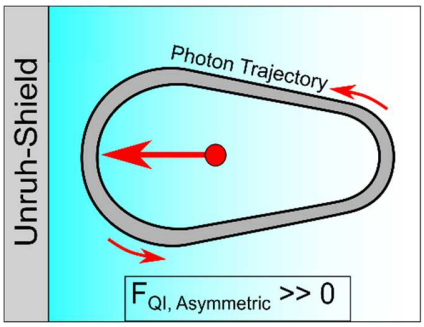

Fig. 17: Proposed thrust generation principle of photons inside an asymmetric fiberoptic loop in presence of an Unruh-shield.

Additional claims McCulloch after our recently reported negative thrust results [4], suggested that the vacuum chamber itself was responsible for the non-existent thrust. Due to its electrically conductive walls surrounding the fiberoptic loop, Unruh radiation is cancelled before interacting with the photons. We therefore decided to retest the device and completely neglect measurement influences by placing the thrust balance on a marble table outside of the vacuum chamber in our lab (fig. 18). We carefully picked a location with the least amount of electrically conductive materials in close proximity of the thrust balance. Especially in front of and behind the fiber-optic coil there were no metallic objects in at least 80 m distance. This way, Unruh waves were not cancelled by anything besides the respective Unruh-shield position close to the loop.

The fiber-optic cable was fed by a semiconducting laser that was directly attached to it. It was supplied by *LUMILOOP* and features a wavelength of 830 nm with up to 1 W of power. It is supplied by a battery-pack and a miniature power supply on the balance. Contrary to previous setups with the Leybold laser-kit, the photons on this setup are created and terminated on the balance itself. This means, that there are no photon momentum exchange with the thrust balance, unlike tests with the silver cavities for example.

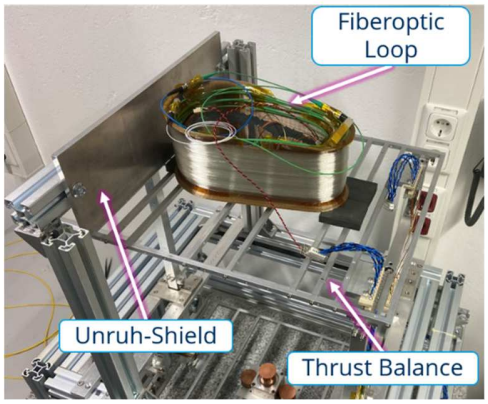

Fig. 18: The asymmetric loop mounted to the thrust balance on a marble table outside of the vacuum chamber with an Unruh-shield close to the bigger radius.

5.5 Fiberoptic Loop – Results & Discussion

With an expected decrease in balance resolution due to atmospheric pressure and convection, we performed three sets of measurements with varying Unruh-shield positions and compared the results.

For force predictions we used the average power between fiber input power and measured power at the end of the 2.2 km fiber to account for losses inside the coil. Two power levels were tested for each of the three Unruh shield positions. At first, the Unruh shield was positioned as close as possible to the big end of the coil. Afterwards the shield was repositioned to the small side of the coil and removed entirely in the third and last test. At average power-levels between laser output- and fiber output-levels of 31 mW and 203 mW with a force amplification factor of 3300, measurements resulted in balance noise only. Even without the protective vacuum environment, we managed to gain a thrust resolution that is below the predicted thrust values with worst-case assumptions by a factor of 14.

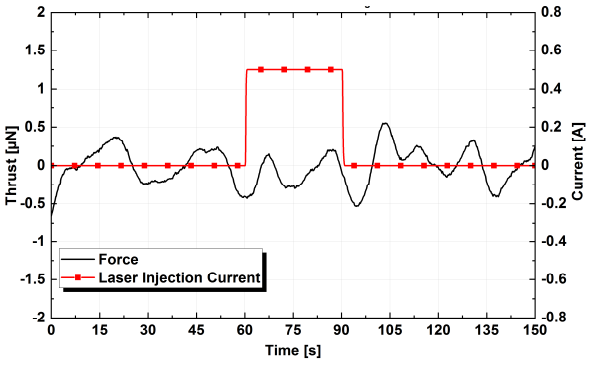

Fig. 19: Thrust measurement of the fiberoptic loop with an Unruh shield close to the small radius and outside of the vacuum chamber with an average power of 203 mW.

No anomalous thrust was detected, as seen in exemplary measurements for the Unruh shield close to the small loop radius in fig 19 and close to the big loop radius in fig. 20. The vacuum chamber did not hide the proposed QI effects.

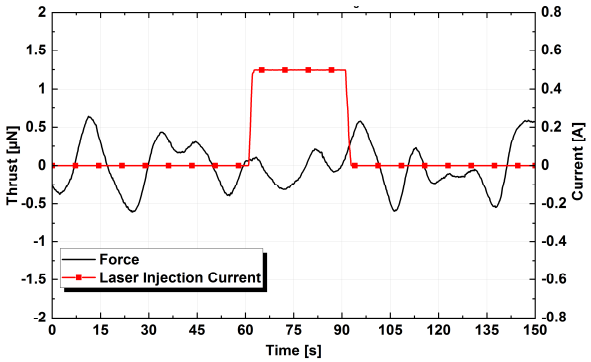

Figure 20: Thrust measurement of the fiberoptic loop with an Unruh shield close to the big radius and outside of the vacuum chamber with an average power of 203 mW.

6. Conclusions

We engaged the recent criticism by the inventors of our devices under test and performed an extended investigation on their proposed concepts.

First, we presented new results on the EMDrive with a refined cavity-geometry utilizing a spherical end-cap rather than flat and removed the dielectric. Four resonance frequencies could be identified in the observed bandwith between 1800 MHz and 2100 MHz with loaded Q-values of up to 1027. Otherwise similar operating conditions, compared to our previous tests with a NASA-like cavity, revealed no anomalous thrust after eliminating the most influential false-positive thrust effects. Also an additional investigation into the inventor's pre-load condition did not change anything.

A second cavity was manufactured involving YBCO high-temperature superconductors to boost predicted thrust values. Initial measurements with a dielectric prevented the formation of superconducting resonance frequencies. Only by removing the dielectric, stable resonances occurred below the critical temperature of 92 K with loaded Q-values of up to 2600. By comparing thrust measurements above and below the critical temperature at selected frequencies, we did not detect any thrust above the balance noise.

Nonetheless, we managed to enhance our thrust balance to operate devices at cryogenic temperatures using solid nitrogen. This allows us to investigate concepts and effects at very low temperatures down to 65 K with sub-micronewton thrust resolution.

Additional thrust measurements of laser-type EMDrives with infrared resonators involved several setup enhancements. The devices underwent hardware changes that supposedly suppressed interactions with emerging Unruh-radiation in our recent null-results.

None of the enhancements in any laser resonator setup revealed anomalous thrust. All measurements stayed within the thrust limit of classical forces due to radiation pressure (Q=1) for the given amount of power.

In summary, we did not encounter unsolvable false-positive thrust signatures in any of our tested devices. Neither the microwave- and superconducting cavities nor the infrared laser resonators passed our requirements for a breakthrough in space propulsion.

Acknowledgements

This work has received support from the German National Space Agency DLR (Deutsches Zentrum für Luft- und Raumfahrttechnik) by funding from the Federal Ministry of Economic Affairs and Energy (BMWi) by approval from German Parliament (50RS1704), as well as from DARPA DSO under award number HR001118C0125.

In addition, we thank M. Kößling for support during the superconducting test campaigns.

References

[1] Tajmar, M., Neunzig, O. & Weikert, M. High-accuracy thrust measurements of the EMDrive and elimination of false-positive effects. *CEAS Space J* (2021). https://doi.org/10.1007/s12567-021-00385-1

[2] Neunzig, O., Weikert, M. & Tajmar, M. Thrust measurements and evaluation of asymmetric infrared laser resonators for space propulsion. *CEAS Space J* (2021). https://doi.org/10.1007/s12567-021-00366-4

[3] Shawyer, R. (2021): Notes on the recent Dresden TU paper. http://emdrive.com/. Accessed 19 Sep 2021.

[4] M. McCulloch (2021) Response to Tajmar's New Cavity Results. . http://physicsfromtheedge.blogspot.com/2021/04/response-to-tajmars-new-cavity-results.html. Accessed 20 Sep 2021.

[5] White, H., March, P., Lawrence, J., Vera, J., Sylvester, A., Brady, D. and Bailey, P.: Measurement of impulsive thrust from a closed radio-frequency cavity in vacuum. J. Propuls. Power **33**(4), 830–841 (2017)

[6] Shawyer, R.: EmDrive Thrust/Load Characteristics. Theory, Experimental Results and a Moon Mission. IAC-19-C4.10.14. 70th International Astronautical Congress, Washington, D.C., 2019

[7] Shawyer, R.: Second generation EmDrive propulsion applied to SSTO launcher and interstellar probe. Acta Astronaut. **116**, 166–174 (2015)

[8] Taylor, T.S.: Propulsive forces using High-Q asymmetric high energy laser resonators. J. Br. Interplanet. Soc. **70**(7), 238–243 (2017)

[9] McCulloch, M.E.: Inertia from an asymmetric Casimir effect. EPL **101**(5), 2013 (2013)

[10] Mcculloch, M.E.: Can the emdrive be explained by quantised inertia? Prog. Phys. **11**(1), 78–80 (2015)

[11] McCulloch, M.E.: Testing quantised inertia on emdrives with dielectrics. Europhys. Lett. **118**(3), 34003 (2017)

Appendix A

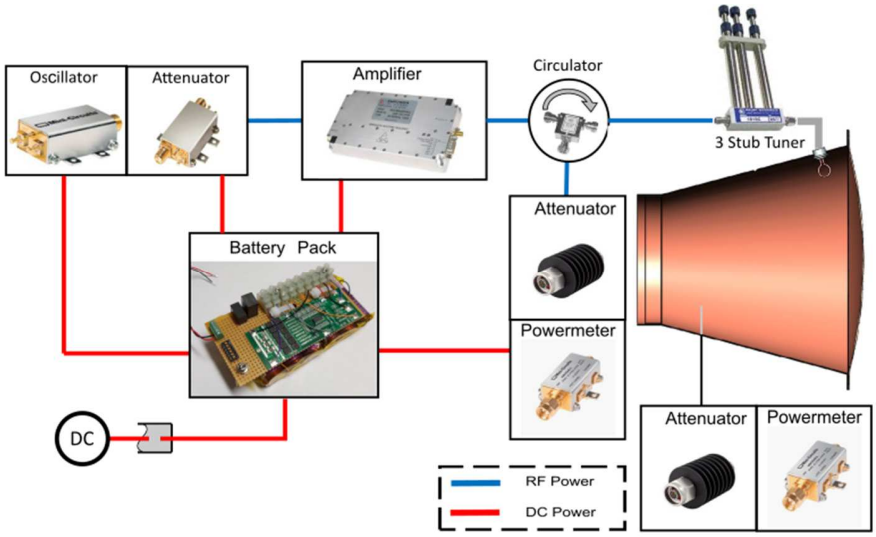

Fig. 21: Electrical Setup of the EMDrive with a spherical end-cap and on-board electronics.

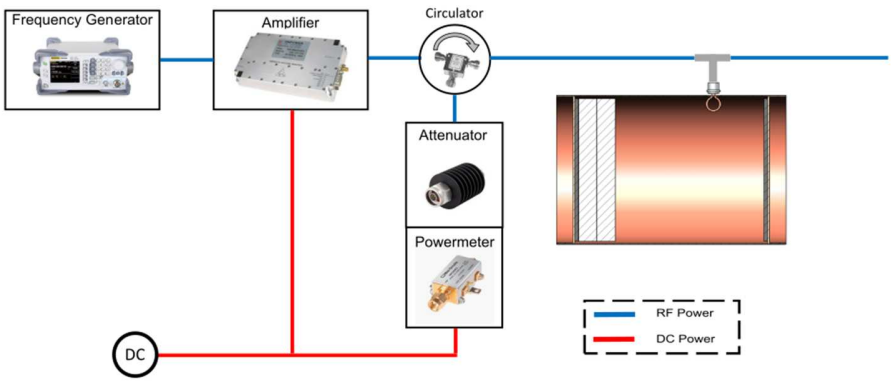

Fig. 22: Electrical setup of the EMDrive with superconducting end-caps with the HF-components outside of the vacuum chamber

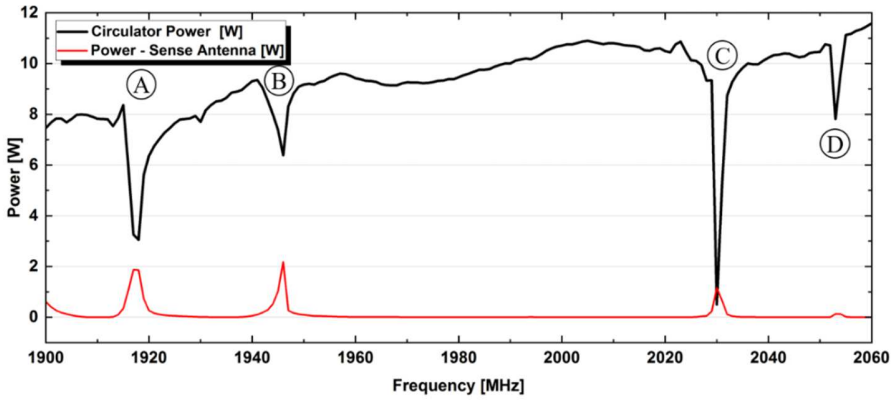

Fig. 23: Spherical EMDrive circulator-power and sense-antenna power measurement between the bandwidth of 1900 MHz-2060 MHz with four resonance frequencies of A) 1918 MHz, B) 1945 MHz, C) 2030 MHz and D) 2054 MHz.

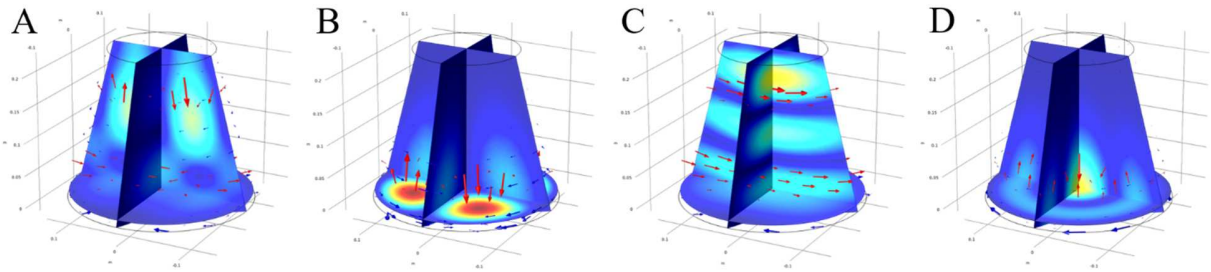

Fig. 24: Simulation of eigenfrequency modes corresponding to frequency peaks in Fig. 22. (A: Hybrid mode, B: TM210, C: TE 113, D: TE020

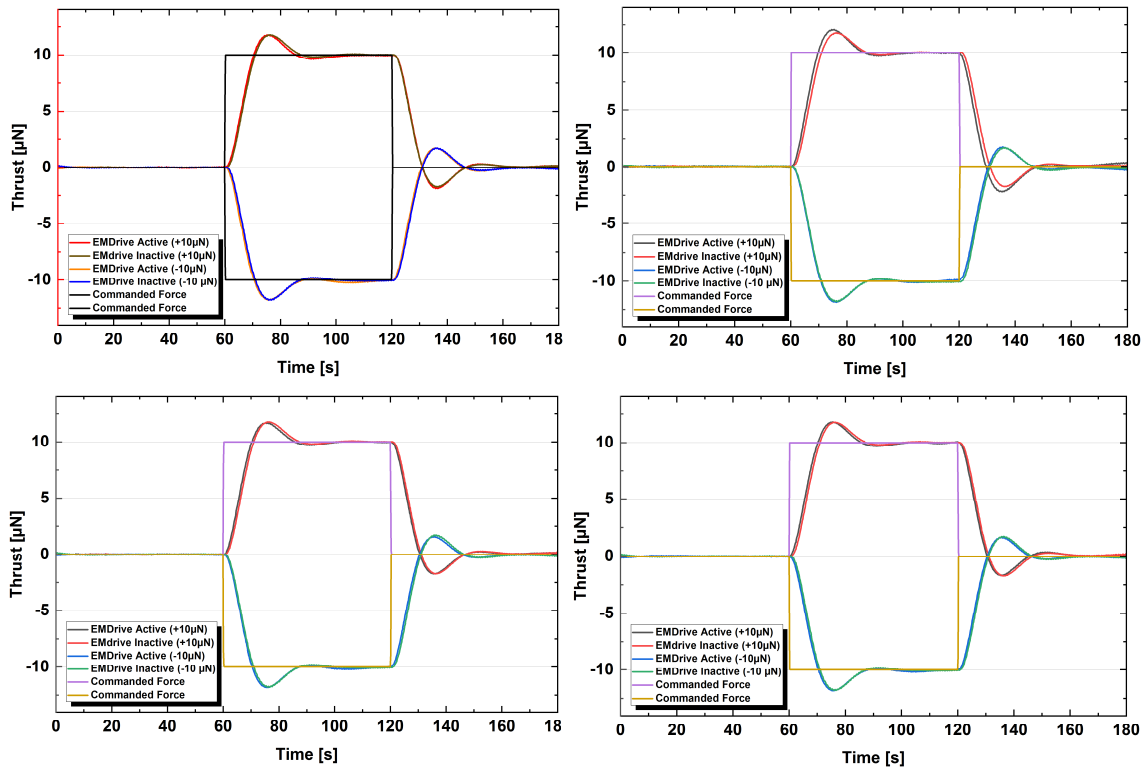

Fig. 25: Thrust measurements of the spherical EMDrive under ± 10µN preload compared to commanded forces of ± 10µN without an operating EMDrive for: A) 1918 MHz, B) 1945 MHz, C) 2030 MHz, D) 2054 MHz.

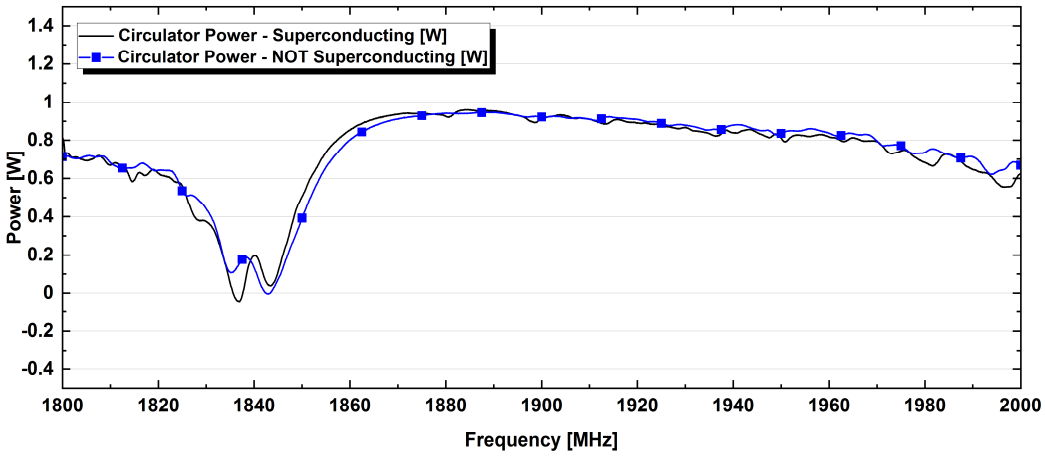

Fig. 27: Comparison of the measured circulator power below and above the critical temperature. No additional resonance frequencies occurred with an active superconductor including the dielectric.

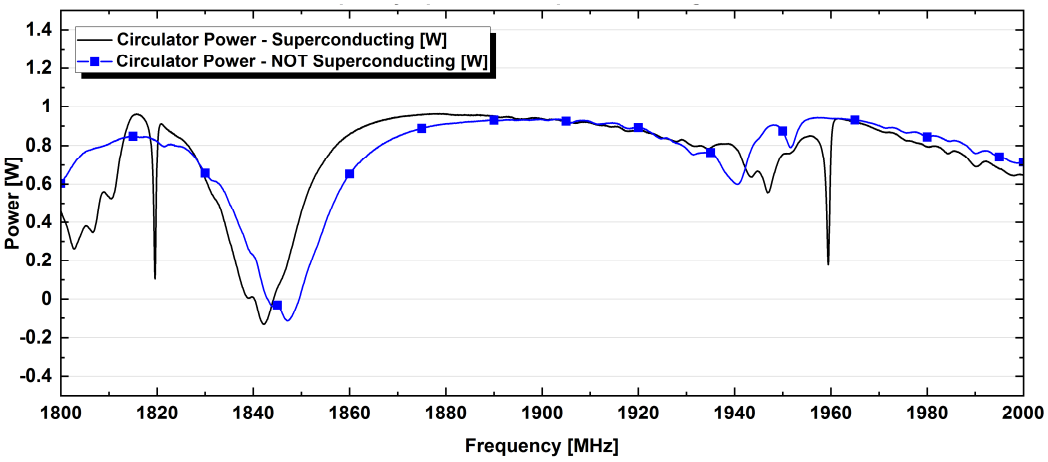

Fig. 26: Comparison of the measured circulator power below and above the critical temperature. Additional SC resonant frequencies occurred only without a dielectric.

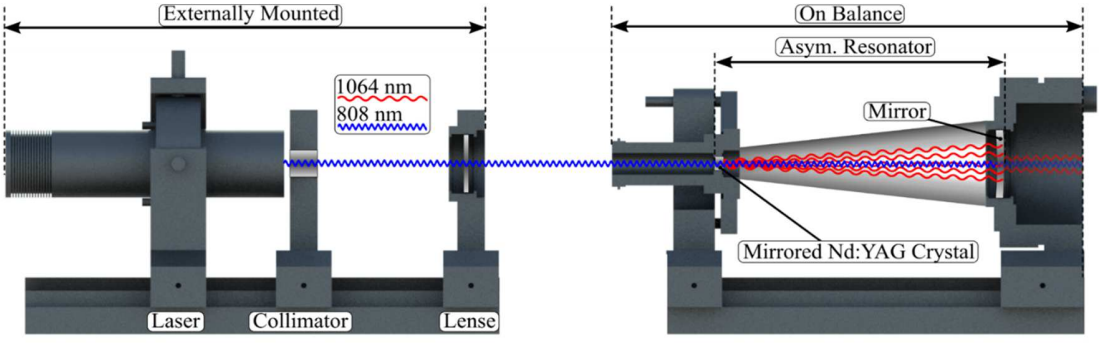

Fig. 28: Illustration of the enhanced Taylor-setup configuration with a tapered metal cavity enclosing the asymmetric laser beam trajectory.

Appendix B (Thrust measurement summary)

Table 1. Thrust measurements of Ag-plated laser resonators.

Setup	Measured Power (P)	QI Force Prediction (F=PS/c)	Classical Photon Thrust (S=1)	Measured Thrust
Beam Trap	279 mW	-	0.93 nN	(0.91 ± 0.31) nN
	467 mW	-	1.56 nN	(1.51 ± 0.15) nN
Concave/Convex (CC/CX)	467 mW	60 nN	1.56 nN	(1.52 ± 0.41) nN
Concave/Concave (CC/CC)	279 mW	36 nN	0.93 nN	(1.04 ± 0.12) nN
	467 mW	60 nN	1.56 nN	(1.65 ± 0.14) nN
Circle	279 mW	36 nN	0.93 nN	(0.89 ± 0.14) nN
	467 mW	60 nN	1.56 nN	(1.50 ± 0.17) nN

Table 2. Thrust measurements of the high-finesse Taylor resonator with a tapered metal cavity surrounding the photon trajectory.

Setup	Measured Power (P)	QI Force Prediction (F=PS/c)	Classical Photon Thrust (S=1)	Measured Thrust
Taylor-Light (+Tapered Cavity)	289 mW	482 nN	0.96 nN	(1.01 ± 0.30) nN
	493 mW	822 nN	1.64 nN	(1.62 ± 0.26) nN

Table 3. Thrust measurements of the asymmetric fiberoptic coil at atmospheric pressure outside of the vacuum chamber.

Setup	Average Fiber Power ($P_{Average}=P_{in}-P_{out}$)	QI Force Prediction (F=PS/c)	Measured Thrust
Fiberoptic coil (No Unruh-shield)	31 mW	0.34 μN	(0.02 ± 0.26) μN
	203 mW	2.23 μN	(0.05 ± 0.30) μN
Fiberoptic coil (Small radius shielded)	31 mW	>0.34 μN	(0.01 ± 0.19) μN
	203 mW	>2.23 μN	(0.09 ± 0.18) μN
Fiberoptic coil (Big radius shielded)	31 mW	>0.34 μN	(0.02 ± 0.15) μN
	203 mW	>2.23 μN	(0.06 ± 0.16) μN

Table 4. Thrust measurements of the EMDrive with a spherical endcap.

Resonance Frequency	$Q_{loaded,S11}$	Measured Power in Cavity (P)	Classical Photon Thrust (Q=1)	Force Prediction (F=PQ/c)	Measured Thrust
1918 MHz	113	6 W	20 nN	2261 nN	(13 ± 31) nN
1945 MHz	486	4.2 W	14 nN	6808 nN	(-7 ± 18) nN
2030 MHz	677	10 W	33 nN	22582 nN	(-4 ± 38) nN
2054 MHz	1027	5.5 W	18 nN	18841 nN	(-11 ± 25) nN

Table 5. Thrust measurements of the superconducting EMDrive.

Resonance Frequency	$Q_{loaded,S11}$	Superconducting	Measured Power in Cavity (P)	Force Prediction (F=PQ/c)	Measured Thrust
1819 MHz	2599	Yes	19 W	164 μN	(0.14 ± 0.23) μN
	-	No	-	-	(0.05 ± 0.24) μN
1959 MHz	2063	Yes	18 W	156 μN	(-0.33 ± 0.54) μN
	-	No	-	-	(0.07 ± 0.08) μN